CrossMark

ORIGINAL PAPER: CHARACTERIZATION METHODS OF SOL-GEL AND HYBRID MATERIALS

# Tailoring the microstructure of $La_{0.6}Sr_{0.4}Co_{0.2}Fe_{0.8}O_{3-\alpha}$ cathode material: the role of dispersing agent

Ismariza Ismail[1] · Nafisah Osman[2] · Abdul Mutalib Md Jani[2]

Abstract A lower operating temperature below 600 °C of the solid oxide fuel cells (SOFCs) is a key determinant of device performance. With this in mind, the roles of dispersing agents were investigated for synthesizing a cathode material made of $La_{0.6}Sr_{0.4}Co_{0.2}Fe_{0.8}O_{3-\alpha}$ (LSCF) for application in intermediate temperature solid oxide fuel cells (IT-SOFCs). In the present study, LSCF was synthesized following a sol–gel method with the aid of an activated carbon and ethylene glycol as dispersing agents. X-ray diffractometer measurements indicate that a single perovskite phase of LSCF started to develop at the temperature of 500 °C and completely formed at 700 °C. Scanning electron microscope analysis confirmed that a well dispersed LSCF powders were successfully synthesized achieving a surface area of 12.05 $m^2\ g^{-1}$ as corroborated by the BET surface area analysis. This finding shows significant improvements of modifying the structural properties of cathode material and could be used to fabricate the next generation of SOFCs.

Graphical Abstract
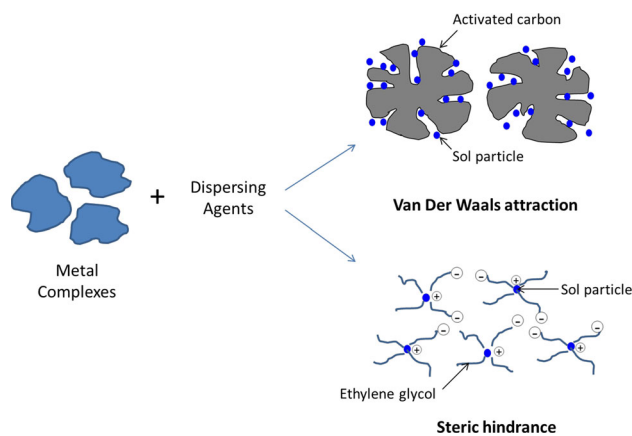
Keywords Cathode material · Modified sol–gel routes · Dispersing agent · Microstructure

1 Introduction

A considerable number of studies have been devoted to the development of solid oxide fuel cell (SOFC) due to its potential as a future power generation system. High operating temperature (800–1000 °C) of SOFC allows fast electrode reaction and mass transport, resulting in high energy conversion efficiency. However, such high operating temperature leads to physical and chemical degradation of the cell and limits the selection of materials that can be used for fabricating SOFC [1, 2]. The need for reducing the SOFC operating temperature in a range of 600–800 °C is imposed by cost reduction, cells' stability and material degradation which is essential for widespread SOFC use [3, 4].

✉ Nafisah Osman
fisha@perlis.uitm.edu.my

1 Faculty of Applied Sciences, Universiti Teknologi MARA, 40450 Shah Alam, Selangor, Malaysia

2 Faculty of Applied Sciences, Universiti Teknologi MARA, Bahagian HEA, STAR Kompleks, 02600 Arau, Perlis, Malaysia

🖄 Springer

In particular, cathode material plays a significant role in lowering the operating temperature associated with the deterioration of electrochemical activity. This event is observed on the perovskite-type manganite-based materials such as LSM ($La_{1-x}Sr_xMnO_{3-\delta}$) that is primarily due to the electrode polarization [5–7]. Accordingly, current research interest is directed toward mixed ionic and electronic conducting (MIEC) materials that exhibit higher ionic conductivities than LSM due to a greater concentration of oxygen vacancies [8, 9]. Among these, lanthanum strontium cobalt ferrite $La_{0.6}Sr_{0.4}Co_{0.2}Fe_{0.8}O_{3-\alpha}$ (LSCF) has been successfully applied to intermediate temperature SOFC (IT-SOFC) due to its high electrical and ionic conductivities as well as excellent chemical and thermal stabilities [10, 11].

Although LSCF is regarded as a good candidate for cathode material due to its intrinsic properties, tailoring the LSCF's structural properties such as porosity and specific surface area allows the improvement of its electrochemical performance [12–14]. Producing the cathode materials with appropriate porosity (20–40 %), small particle size and high surface area is desirable as it will extend the triple-phase boundaries (TPBs) active area, where the electrochemical reaction occurs [13, 15]. With this improvement, the cathode material would exhibit high electrical conductivity and good catalytic activity and therefore, superior cell performance [16–18]. Previous related works are mostly focused on the synthesizing techniques and formulations of cathode materials that are sometimes costly, tedious and time-consuming [19–21].

The very limited study has been centered on the application of additive and synthesizing aid such as a dispersing agent, and its role in optimizing the microstructure is scarcely discussed [9, 17, 22]. Although carbon black has been used as dispersing agent to synthesize LSCF in [17], the complete formation of the single-phase powder was only achieved after calcination over 700 °C. To the author's best knowledge, there is no effort reporting the use of activated carbon for synthesizing LSCF has a single-phase calcination temperature below 700 °C.

In this study, LSCF-based cathode materials are prepared by a sol–gel method using ethylenediaminetetraacetic acid (EDTA) and citric acid as chelates. The dispersing agents such an activated carbon or ethylene glycol are used in the synthesizing process in order to control the distribution and particle size of the cathode materials. Activated carbon is a treated form of carbon which possesses millions of tiny pores and well known for its high surface area (300–2000 m^2/g). Due to its high degree of microporosity and well-adsorption ability, the activated carbon was applied as the dispersing agent in this study to investigate the effect of the micropores on the formation of the cathode particles. As for comparison,

ethylene glycol which has been used as the dispersant in [9] was also applied as the dispersing agent and its role in inducing dispersibility of the cathode particles is further investigated. Microstructural analysis was performed to verify the properties of the best obtained cathode materials and, subsequently, was compared with the material synthesized without the aids of a dispersing agent.

2 Experimental details

The general procedure for synthesizing $La_{0.6}Sr_{0.4}Co_{0.2}Fe_{0.8}O_{3-\alpha}$ (LSCF) is schematically shown in Fig. 1. The precursor solution was prepared by dissolving the stoichiometric composition of $La(NO_3)_3.6H_2O$ (99.9 %, ACROS), $Sr(NO_3)_2$ (99 %, ACROS), $Co(NO_3)_2.6H_2O$ (99 %, ACROS) and $Fe(NO_3)_3.9H_2O$ (99 %, ACROS) in 100 ml of deionized water. After complete dissolution of the salts, citric acid monohydrate (CA) (99.5 %, MERCK) was introduced into the nitrate solution, followed by ethylenediaminetetraacetic acid (EDTA) (99 %, ACROS). The mixture was then heated in 70 °C water bath under continuous stirring. CA and EDTA powders served as the raw materials for chelation process. The obtained clear solution was mixed with the dispersing agents to promote dispersion and prevent clumping of resulting cathode materials. Two types of dispersing agents were employed in the synthesizing process which is charcoal activated carbon (HmbG) and ethylene glycol (ACROS). Samples prepared with different types of dispersing agents are shown in Table 1. The mixture was continuously stirred
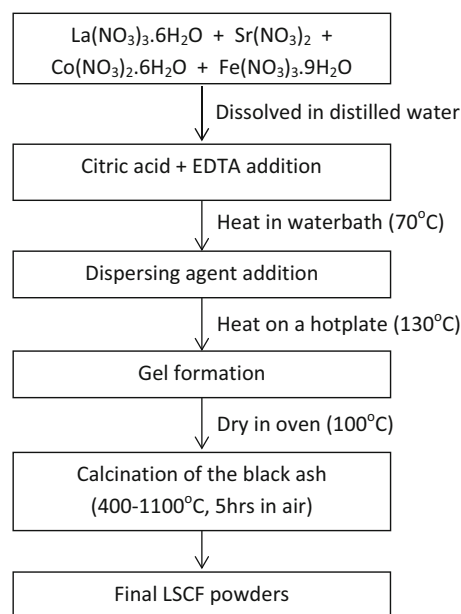

Fig. 1 Synthesis steps of LSCF materials by a complexing method

Table 1 Batches of La$_{0.6}$Sr$_{0.4}$Co$_{0.2}$Fe$_{0.8}$O$_{3-\alpha}$ cathode powders

Sample ID	Dispersing agent (DA)	Molar ratio of DA/LSCF
LSCF64 (pristine)	–	–
LSCF-AC03	Activated carbon	0.3
LSCF-AC07	Activated carbon	0.7
LSCF-EG03	Ethylene glycol	0.3
LSCF-EG07	Ethylene glycol	0.7

and heated to evaporate the water. The resulting viscous gel was dried at 100 °C in a vacuum oven overnight, and the solidified precursor was then crushed and calcined at 400–1100 °C for 5 h to promote the formation of LSCF perovskite phase. Phase formation of the oxide compound was verified by X-ray diffractometer (XRD) (PANalytical X'Pert PRO MRD PW3040), employing Cu–K$_\alpha$ radiation from 20° to 80° in the step of 0.05° at 2θ. The phase formation analysis was performed by using Eq. 1 as proposed by Swarts and Shrout [23]:

$$\text{Perovskite phase} = \frac{I_p}{I_p + I_m} \times 100\,\% \qquad (1)$$

where I_p refers to the maximum intensity of the perovskite phase and I_m is the maximum intensity of the impurities phases. The lattice constant of the samples was calculated using an indexing method based on Bragg's law with the assistance of a Mathcad 14 software [24].

Field emission scanning electron microscopy (FESEM) (Nova NANO-SEM 450) equipped with Oxford X-Max^N energy-dispersive X-ray system was employed to observe the microstructures and elemental composition of the LSCF. The micrographs obtained were used to estimate the particle size and the morphology of the sample using an image analysis system (ImageJ 1.45p). The reflection from the (020) plane was used to estimate the average of crystallite size, D. The D value was calculated from the Scherrer formula as in Eq. 2:

$$D = 0.9\lambda/(\beta \cos\theta) \qquad (2)$$

where λ is the X-ray wavelength, β is the line broadening at half the maximum intensity (FWHM) and θ refers to the Bragg angle. Finally, the specific surface area of the LSCF was obtained using BET analyzer (Quantachrome Autosorb AS1C).

3 Results and discussion

3.1 XRD analysis

Figure 2 shows X-ray diffraction patterns of LSCF prepared with the addition of activated carbon and ethylene glycol after calcination at 400–1100 °C for 5 h. The profile presented characteristic peaks of the perovskite LSCF
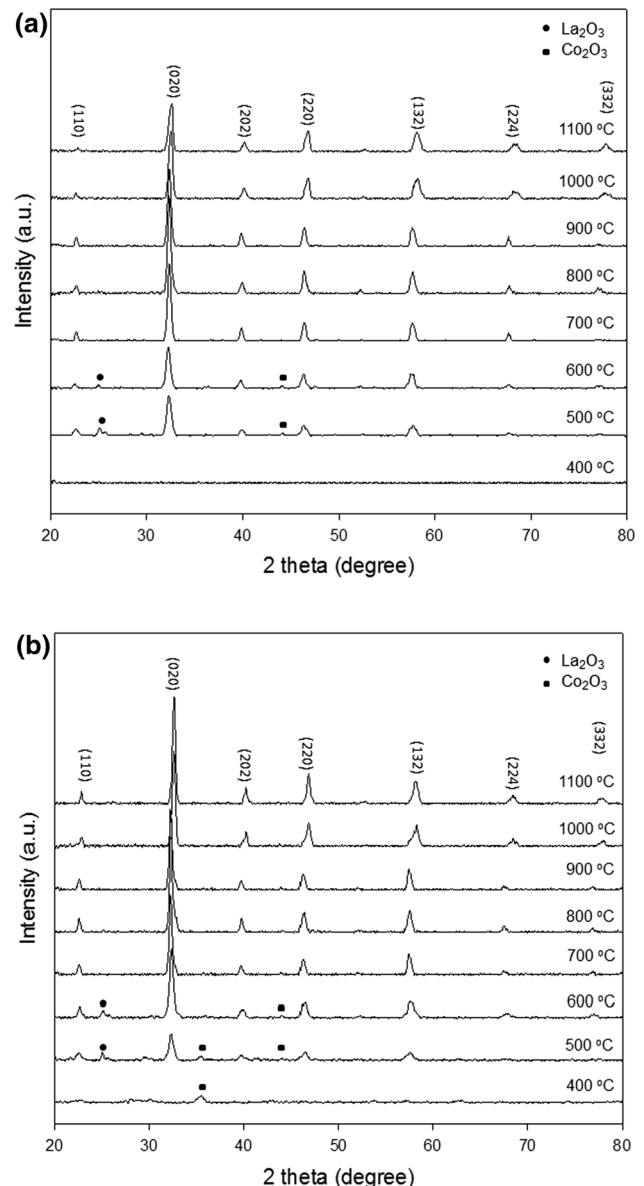

Fig. 2 XRD patterns of **a** LSCF-AC07 and **b** LSCF-EG07 cathode materials as function of calcination temperatures

phase appears in both samples of cathode materials after the calcination process at 500 °C. No secondary phases are observed, and close observation of Fig. 2a, b reveals the appearance of two small peaks at 2$\theta \approx$ 26° and 44° which

are the main peaks of La_2O_3 and Co_2O_3, respectively. However, the impurities peaks disappear as the calcination temperature increased and the complete formation of a single perovskite LSCF phase with orthorhombic structure is achieved at 700 °C (JCPDS 89-1268). The pronounce peaks can be indexed to their Miller indices (hkl) of (110), (020), (202), (220), (132), (224) and (332), accordingly. Figure 3 shows the XRD pattern of LSCF samples prepared at different concentrations of activated carbon and ethylene glycol after calcined at 700 °C. A well-crystalline perovskite phase of LSCF in all samples appeared at
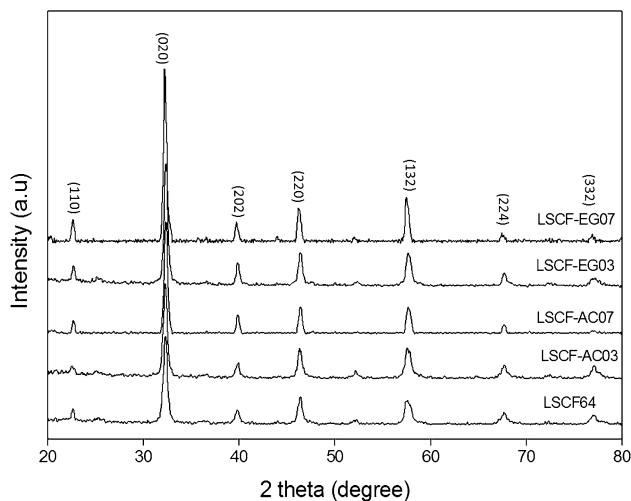

Fig. 3 XRD patterns of the cathode materials prepared using different concentrations of activated carbon and ethylene glycol after calcined at 700 °C

700 °C, which is at a relatively lower temperature compared with the temperature over 900 °C prepared by combustion and other synthesis methods [9, 20, 25].

The percentages of the perovskite phase for the LSCF prepared at various calcination temperatures are presented in Table 2. It was observed that the percentage of the perovskite phase increase with the increase in calcination temperature and a complete formation of a perovskite phase were obtained after a calcination process at 700 °C. Additionally, the purity of the LSCF phase was preserved even after thermal treatment at 1100 °C, suggesting that the compound remains stable even at elevated temperatures. The lattice constant calculated for the LSCF prepared by introducing different dispersing agents as a function of calcination temperature is illustrated in Fig. 4. The values obtained were in agreement with JCPDS 89-1268 for LSCF ($a = 5.4750$ Å; $b = 5.5360$ Å; $c = 7.7691$ Å). No large-scale change in lattice constant with increasing calcination temperatures can be explained on the basis of phase stability. The crystallite size of the untreated sample, as well as samples prepared with different dosage of dispersing agents at 700 °C, was determined using Scherrer equation and presented in Table 3. The crystallite size of LSCF obtained was relatively similar for all samples which are around 19 nm. The addition of dispersing agents during the synthesizing process seems to retain the crystallite growth of the sample. This observation was also supported by XRD spectra obtained, showing no significant changes in the peak position of the LSCF as a function of activated carbon and ethylene glycol. Thus, it can be concluded that

Table 2 Phase formation analysis of the cathode samples

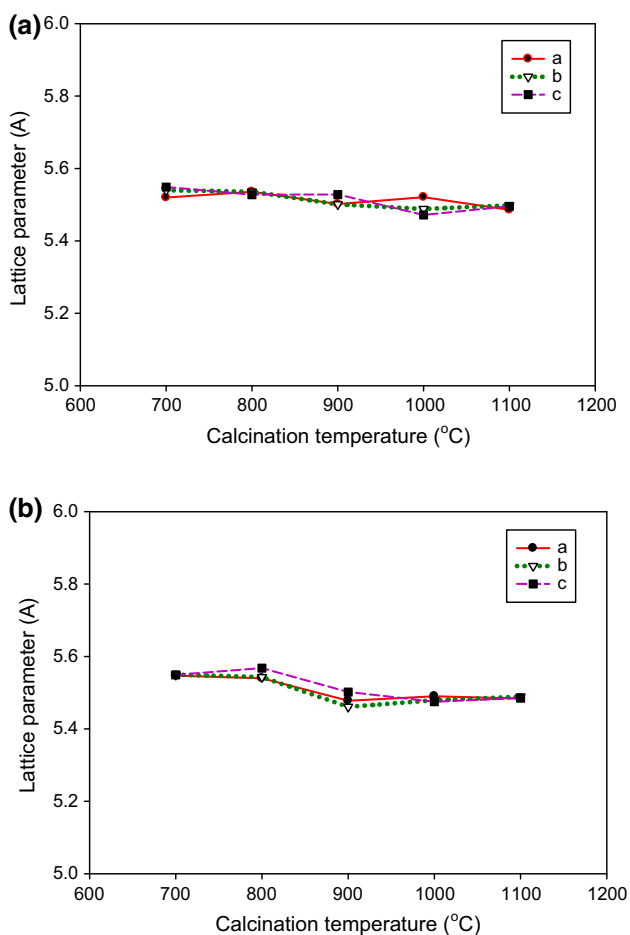| Sample	Calcination temperature (°C)	Crystalline phases	Amount of each phase (%)	
			Perovskite	Impurity
LSCF-AC07	400	La_2O_3, Co_2O_3	–	100
	500	$La_{0.6}Sr_{0.4}Co_{0.2}Fe_{0.8}O_{3-\alpha}$, La_2O_3, Co_2O_3	84	16
	600	$La_{0.6}Sr_{0.4}Co_{0.2}Fe_{0.8}O_{3-\alpha}$, La_2O_3, Co_2O_3	93	7
	700	$La_{0.6}Sr_{0.4}Co_{0.2}Fe_{0.8}O_{3-\alpha}$	100	–
	800	$La_{0.6}Sr_{0.4}Co_{0.2}Fe_{0.8}O_{3-\alpha}$	100	–
	900	$La_{0.6}Sr_{0.4}Co_{0.2}Fe_{0.8}O_{3-\alpha}$	100	–
	1000	$La_{0.6}Sr_{0.4}Co_{0.2}Fe_{0.8}O_{3-\alpha}$	100	–
	1100	$La_{0.6}Sr_{0.4}Co_{0.2}Fe_{0.8}O_{3-\alpha}$	100	–
LSCF-EG07	400	$La_{0.6}Sr_{0.4}Co_{0.2}Fe_{0.8}O_{3-\alpha}$, La_2O_3, Co_2O_3	28	72
	500	$La_{0.6}Sr_{0.4}Co_{0.2}Fe_{0.8}O_{3-\alpha}$, La_2O_3, Co_2O_3	77	23
	600	$La_{0.6}Sr_{0.4}Co_{0.2}Fe_{0.8}O_{3-\alpha}$, La_2O_3, Co_2O_3	91	9
	700	$La_{0.6}Sr_{0.4}Co_{0.2}Fe_{0.8}O_{3-\alpha}$	100	–
	800	$La_{0.6}Sr_{0.4}Co_{0.2}Fe_{0.8}O_{3-\alpha}$	100	–
	900	$La_{0.6}Sr_{0.4}Co_{0.2}Fe_{0.8}O_{3-\alpha}$	100	–
	1000	$La_{0.6}Sr_{0.4}Co_{0.2}Fe_{0.8}O_{3-\alpha}$	100	–
	1100	$La_{0.6}Sr_{0.4}Co_{0.2}Fe_{0.8}O_{3-\alpha}$	100	–

Fig. 4 Lattice constant of **a** LSCF-AC07 and **b** LSCF-EG07 as a function of calcination temperatures. Lattice constant c is divided by $\sqrt{2}$ for comparison with **a**, **b**

Table 3 Crystallite size of LSCF samples after calcined at 700 °C

Sample ID	2θ	β_{FWHM}	Crystallite size (nm)[a]
LSCF64	32.291	0.420	19.7
LSCF-AC03	32.247	0.443	18.7
LSCF-AC07	32.339	0.420	19.7
LSCF-EG03	32.338	0.394	19.9
LSCF-EG07	32.204	0.420	19.7

[a] Estimated value only because the size was calculated from the total line broadening due to the limitation of XRD measurement

phase formation of LSCF is practically not affected by the addition of dispersing agents which are in agreement with other reported work published elsewhere [17, 26].

3.2 SEM/EDX characterization

Figure 5 presents the SEM images of the LSCF powders with the addition of activated carbon and ethylene glycol

heated at 700 °C in the air. The aggregates of several primary particles with spherical in shape were observed in all samples. The particle size distribution of the LSCF powders is quite narrow, and the averaged size is in the range of 10–60 nm. The occurrence of a coarsened microstructure was most prominent for the untreated sample (Fig. 5a). Fewer coarse particles were observed for samples prepared with an addition of activated carbon and ethylene glycol as the synthesizing aid (Fig. 5b–e). The size of particles measured for the LSCF64 sample is in the range of 60–300 nm whereas, for both samples prepared using dispersing agents, the particle size measured is relatively smaller in the range of 40–200 nm.

With the addition of 0.3 molar ratio of dispersing agent/ LSCF, it is noticeable that the powders are well dispersed and smaller amount coarse particles were observed (Fig. 5b, c). The homogeneity of LSCF powder improved after adding 0.7 molar ratio of dispersing agent/LSCF with the formation of a less coarsened microstructure (Fig. 5d, e). This was more pronounced in the sample prepared with an ethylene glycol (Fig. 5e). It was found that the addition of dispersing agent during the synthesizing process had a significant effect on the morphology of the LSCF powders. The LSCF powders synthesized without dispersing agent tend to form a micron-scaled particle.

The average particle size for all sample batches measured using SEM image analysis software is summarized in Table 4. The particle size obtained by SEM measurements for each sample differs from the crystallite size obtained from XRD measurements (Table 3) as discussed in the previous section. The differences in these two measurements values are expected because the particle may be composed of several different crystallites [27].

The proposed mechanisms of the reaction involved during the synthesizing process using both dispersing agents are illustrated in Fig. 6. As shown in Fig. 6a, activated carbon served as a suitable dispersing agent by trapping the metal complexes in its highly porous microstructure. The improvement in the LSCF microstructure upon addition of a dispersing agent is attributed to van der Waals attraction creating well-dispersed cathode particles after sintering process. On the other hand, the addition of ethylene glycol to the precursor solution acts as a stabilizer to prevent agglomeration of particles due to the influence of its high surface energy. During the steric stabilization process, ethylene glycol will undergo polymerization with metal complexes and formed a coating-like structure that creates a repulsive force and prevents aggregates from occurring as shown in Fig. 6b.

This step explains the smaller particle size of LSCF powders synthesized by ethylene glycol as compared to those prepared using activated carbon. In the subsequent heating process, the gasses liberated hinder or limit the
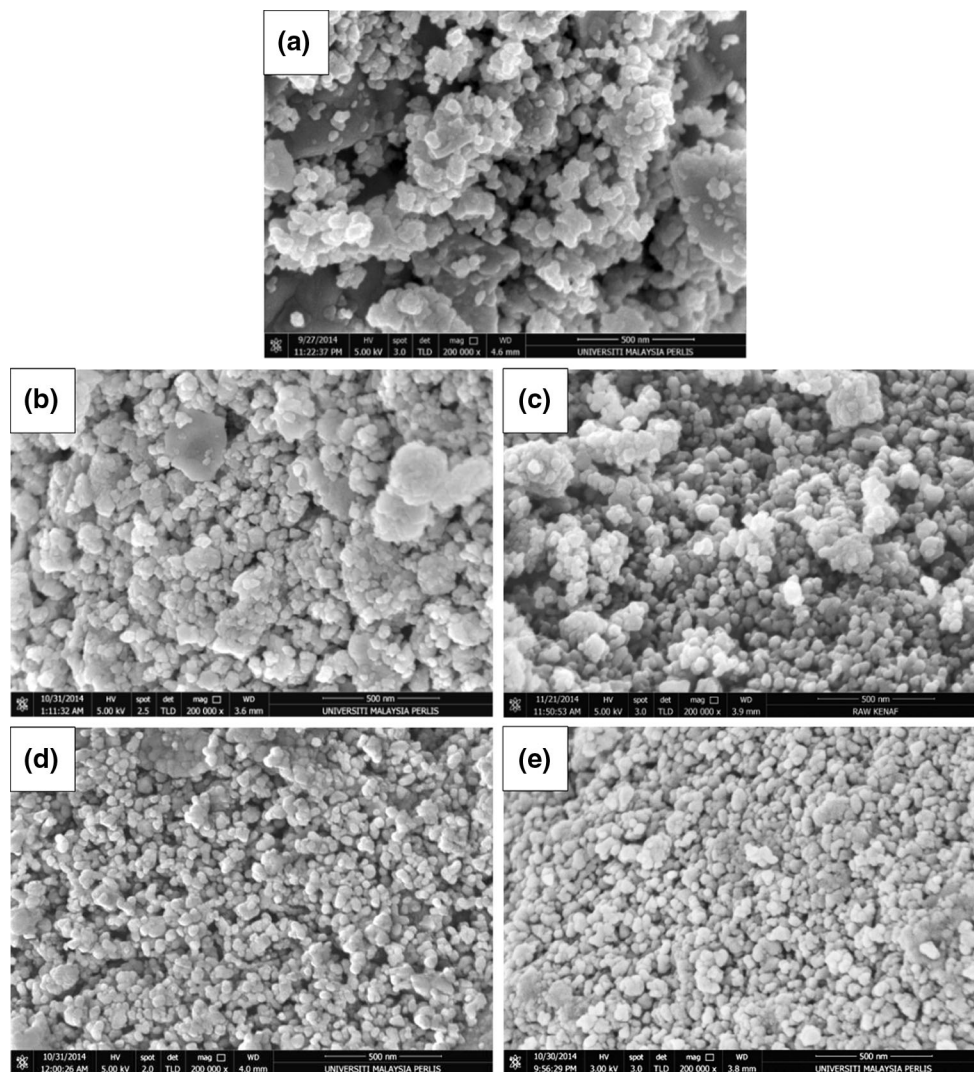
Fig. 5 FESEM images of **a** LSCF64, **b** LSCF-AC03, **c** LSCF-EG03, **d** LSCF-AC07 and **e** LSCF-EG07 cathode materials after calcined at 700 °C for 5 h

Table 4 Average particle size of LSCF samples measured by SEM image analysis software

Sample ID	Average particle size (nm)
LSCF64	38.4
LSCF-AC03	37.1
LSCF-AC07	36.1
LSCF-EG03	35.4
LSCF-EG07	34.1

degree of the inter-particle contact which then allows the nucleation process to occur through the rearrangement and a short distance diffusion of nearby atoms or molecules. As a result, the initial nanosize of the particle was retained after the heat treatment process [28].

The elemental mapping performed by energy-dispersive X-ray (EDX) pattern is presented in Fig. 7. For clarity, only the EDX pattern for LSCF64 sample is presented in the figure but similar patterns were obtained for all samples prepared. Clearly, seen peaks for La, Sr, Co, Fe and O are observed, showing that these five elements are present in all sample batches as per expectation. The quantification of the different elements in terms of the atomic percentage shown in Table 5 confirms these results. In summary, activated carbon and ethylene glycol served as an excellent synthesizing aid in preventing agglomeration and these observations are in accordance with previous work implementing another type of dispersing agent [17, 26].
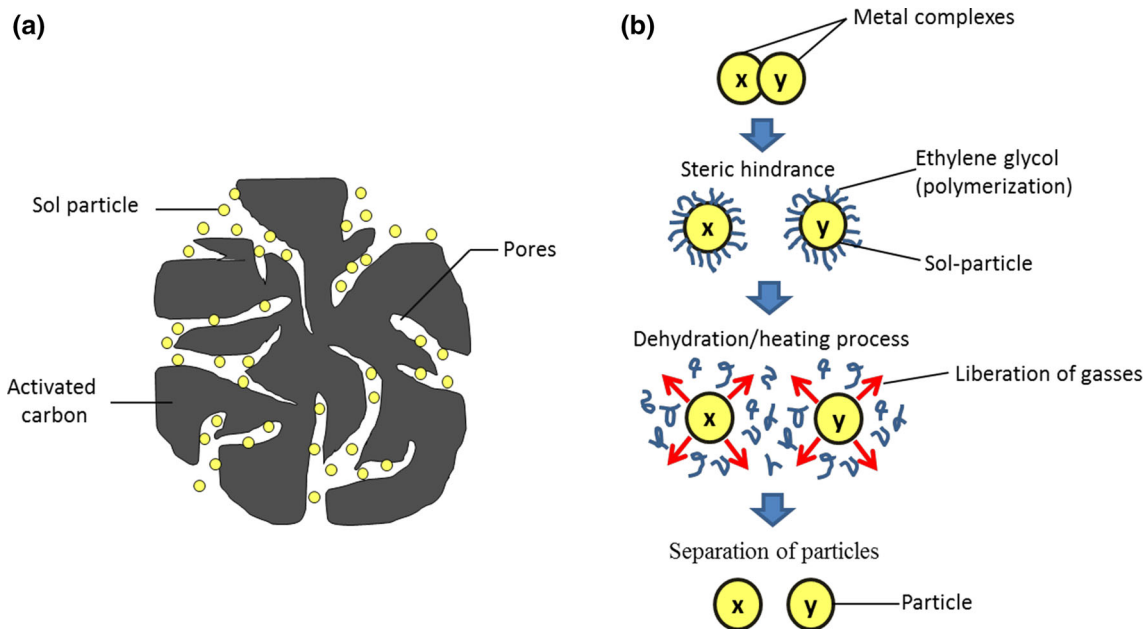
Fig. 6 Schematic diagram of the possible process involved in producing fine-particle powders using **a** activated carbon and **b** ethylene glycol (*Note*: adapted from [28, 30])
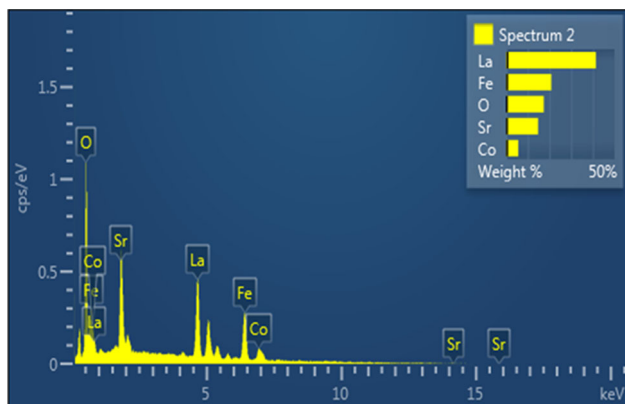

Fig. 7 EDX analysis of LSCF64 sample prepared at 700 °C

Table 5 Atomic percentage for the element of interest quantified from EDX pattern of LSCF64 sample

Element	O	La	Sr	Co	Fe	Total
Atomic percentage	17.43	41.40	14.72	5.62	20.83	100.00

3.3 Surface area analysis

The specific surface area of the cathode samples was investigated by nitrogen adsorption and desorption measurements. The results are summarized in Table 6. The surface areas measured for the sample prepared with the aid of the dispersing agents are noticeably higher as compared to the untreated sample. For cathode samples prepared with

Table 6 Surface area of the $La_{0.6}Sr_{0.4}Co_{0.2}Fe_{0.8}O_{3-\alpha}$ powder after calcined at 700 °C

Sample ID	BET surface area (m^2 g^{-1})
LSCF64	7.4
LSCF-AC03	10.0
LSCF-AC07	11.0
LSCF-EG03	9.5
LSCF-EG07	12.0

the addition of 0.3 molar ratio of dispersing agent/LSCF, the surface areas of both samples are almost identical. However, when the molar ratio of the dispersing agent/LSCF increased to 0.7, the surface area for the sample prepared with ethylene glycol is relatively higher as compared to the one made by activated carbon. The BET results are in accordance with the morphologies of LSCF powders obtained from SEM images as discussed in a previous section. The surface areas obtained are comparatively higher than those reported for powders prepared by different formulations as summarized in Table 7. The lower surface area obtained in other reported works might be explained by the formation of agglomerates or coarse particles during the synthesizing process due to the absence of the dispersing agent. This might be because, during the combustion process when the organic compounds were removed, the metal ions reacted with each other to form LSCF particle without any restraint, and consequently, the particles tend to bind to each other and cause the aggregation. Thus, limited surface areas are available for the

Table 7 Comparison of the surface area for LSCF cathode powders prepared by different methods

Compound	Method	BET surface area ($m^2 \ g^{-1}$)	References
$La_{0.4}Sr_{0.6}Co_{0.8}Fe_{0.2}O_{3-\delta}$	Acetate method	8.3	[29]
$La_{0.6}Sr_{0.4}Co_{0.2}Fe_{0.8}O_{3-\delta}$	Citrate method	5.5	[12]
$La_{0.6}Sr_{0.4}Co_{0.2}Fe_{0.8}O_{3-\delta}$	Citrate-hydrothermal method	5.2	[20]
$La_{0.6}Sr_{0.4}Co_{0.2}Fe_{0.8}O_{3-\delta}$	Dispersing agent-assisted sol–gel method	12.0	[This work]

corresponding reaction. On the other hand, dispersing agent used in this case can provide excellent steric and electrostatic stabilization and creates the formation of smaller and well-dispersed LSCF particles with a higher surface area.

4 Conclusions

In this work, LSCF cathode materials have been synthesized by the addition of dispersing agent through a modified sol–gel method. Two different types of dispersing agents were selected, and they are activated carbon and ethylene glycol. The complete formation of single-phase LSCF was attained at 700 °C for all samples prepared with the help of dispersing agents. The LSCF powders prepared by introducing the dispersing agent into the sol exhibit superior properties in terms of microstructure and surface area as compared to the untreated sample. The morphology of LSCF powder prepared by the addition of ethylene glycol shows relatively smaller particle size as compared to activated carbon. The observation from SEM analysis is in accordance with the BET results in which higher surface area was obtained for the sample prepared with these synthesizing aids. These results indicated that the addition of dispersing agents during the cathode synthesizing process is one of the critical parameters in producing a small particle size and a high surface area of nanocrystalline cathode materials for IT-SOFCs application. More importantly, the result was also useful in finding new effective and suitable dispersant for synthesizing cathode materials. The effect of dispersing agent addition on the electrochemical performance of the prepared cathode powders will be published elsewhere.

References

1. Ortiz-Vitoriano N, Bernuy-López C, Ruiz de Larramendi I, Knibbe R, Thydén K, Hauch A, Holtappels P, Rojo T (2013) Appl Energy 104:984–991

2. Ding Z, Yang Z, Zhao D, Deng X, Ma G (2013) J Alloy Compd 550:204–208

3. Ricote S, Bonanos N, Rørvik PM, Haavik C (2012) J Power Sources 209:172–179

4. Peng R, Wu T, Liu W, Liu X, Meng G (2010) J Mater Chem 20:6218–6225

5. Qiang F, Sun K, Zhang N, Le S, Zhu X, Piao J (2009) J Solid State Electrochem 13:455–467

6. Wu L, Jiang Z, Wang S, Xia C (2013) Int J Hydrogen Energy 38:2398–2406

7. Yu H-C, Fung K-Z (2003) Mater Res Bull 38:231–239

8. Dusastre V, Kilner J (1999) Solid State Ionics 126:163–174

9. Ghouse M, Al-Yousef Y, Al-Musa A, Al-Otaibi MF (2010) Int J Hydrogen Energy 35:9411–9419

10. Zhao E, Liu X, Liu L, Huo H, Xiong Y (2014) Prog Nat Sci Mater Int 24:24–30

11. Hu B, Wang Y, Xia C (2014) J Power Sources 269:180–188

12. Murata K, Fukui T, Abe H, Naito M, Nogi K (2005) J Power Sources 145:257–261

13. da Conceição L, Silva AM, Ribeiro NFP, Souza MMVM (2011) Mater Res Bull 46:308–314

14. Ortiz-Vitoriano N, Ruiz de Larramendi I, Gil de Muro I, Ruiz de Larramendi JI, Rojo T (2010) Mater Res Bull 45:1513–1519

15. Singhal SC, Kendall K (2003) High-temperature solid oxide fuel cells: fundamentals, design and applications. Elsevier, New York

16. Zhou W, Shao Z, Jin W (2006) J Alloy Compd 426:368–374

17. Kim JH, Park YM, Kim H (2011) J Power Sources 196:3544–3547

18. Sun C, Hui R, Roller J (2009) J Solid State Electrochem 14:1125–1144

19. Letilly M, Joubert O, Le Gal La Salle A (2012) J Power Sources 212:161–168

20. Garcia LMP, Macedo DA, Souza GL, Motta FV, Paskocimas CA, Nascimento RM (2013) Ceram Int 39:8385–8392

21. Liu Z, Liu M, Nie L, Liu M (2013) Int J Hydrogen Energy 38:1082–1087

22. Mazlan NA, Osman N, Jani AMM, Yaakob MH (2015) J Sol–Gel Sci Technol 78:50–59

23. Wongmaneerung R, Yimnirun R, Ananta S (2009) Mater Chem Phys 114:569–575

24. Erb T, Zhokhavets U, Gobsch G, Raleva S, Stühn B, Schilinsky P, Waldauf C, Brabec CJ (2005) Adv Funct Mater 15:1193–1196

25. Chanquía CM, Mogni L, Troiani HE, Caneiro A (2014) J Power Sources 270:457–467

26. Jin HW, Kim JH, Park YM, Choi C, Kim H-J, Kim H (2012) J Ceram Process Res 13:S286–S290

27. Itoh T (1985) J Mater Sci Lett 4:431–433

28. Tao Y, Shao J, Wang J, Wang WG (2008) J Power Sources 185:609–614

29. Baqué L, Caneiro A, Moreno MS, Serquis A (2008) Electrochem Commun 10:1905–1908

30. Nambam JS, Philip J (2012) J Colloid Interface Sci 366:88–95